WILEY

Characterization of a temporoparietal junction subtype of Alzheimer's disease

François Meyer[1] | Marie Wehenkel[1,2] | Christophe Phillips[1] | Pierre Geurts[2] | Roland Hustinx[3] | Claire Bernard[3] | Christine Bastin[1] | Eric Salmon[1] | the Alzheimer's Disease Neuroimaging Initiative[†]

[1]GIGA-Cyclotron Research Centre in vivo imaging, University of Liège, Liège, Belgium

[2]Department of Electrical Engineering and Computer Science, University of Liège, Liège, Belgium

[3]Nuclear Medecine Department, CHU of Liège, University of Liège, Liège, Belgium

Correspondence
François Meyer, Cyclotron Research Centre, Quartier Agora, B30 Sart Tilman, Allée de Six-Août 8, Liège 4000, Belgium.
Email: francois.meyer@chuliege.be

Abstract

Alzheimer's disease (AD) subtypes have been described according to genetics, neuropsychology, neuropathology, and neuroimaging. Thirty-one patients with clinically probable AD were selected based on perisylvian metabolic decrease on FDG-PET. They were compared to 25 patients with a typical pattern of decreased posterior metabolism. Tree-based machine learning was used on those 56 images to create a classifier that was subsequently applied to 207 Alzheimer's Disease Neuroimaging Initiative (ADNI) patients with AD. Machine learning was also used to discriminate between the two ADNI groups based on neuropsychological scores. Compared to AD patients with a typical precuneus metabolic decrease, the new subtype showed stronger hypometabolism in the temporoparietal junction. The classifier was able to distinguish the two groups in the ADNI population. Both groups could only be distinguished cognitively by Trail Making Test-A scores. This study further confirms that there is more than a typical metabolic pattern in probable AD with amnestic presentation.

KEYWORDS
Alzheimer, FDG-PET, machine learning, neuroimaging, subtypes

1 | INTRODUCTION

Alzheimer's disease (AD) is known as the primary cause of dementia worldwide. With the growing knowledge of AD biomarkers and physiopathology of the disease (Jack Jr. et al., 2016), diagnostic criteria have evolved to obtain a common and reliable disease definition that can be used in both research and clinical practice (McKhann et al., 2011). However, it has also long been known that AD is a composite disease with heterogeneous subtypes in terms of genetics, with more than 20 loci

described as part of the pathophysiology (Karch & Goate, 2015), with early and late age at onset, characterized by difference in distribution of cortical hypometabolism (Frisoni et al., 2005; Kim et al., 2005), and different clinical presentations, with amnestic, posterior cortical atrophy, progressive primary aphasia, and frontal variants (Alladi et al., 2007; Galton, Patterson, Xuereb, & Hodges, 2000). Even within the typical amnestic presentation, there is heterogeneity in cognitive profiles (Fisher, Rourke, & Bieliauskas, 1999; Lambon, Patterson, Graham, Dawson, & Hodges, 2003; Stopford, Snowden, Thompson, & Neary, 2008; Strite, Massman, Cooke, & Doody, 1997; Vardy et al., 2013) and patterns of cortical hypometabolism of patients (Salmon et al., 2009).

Among the many tools used in the diagnosis and classification of AD, Positron Emission Tomography with [18F]fluorodeoxyglucose (FDG-PET) is one of the most common neuroimaging technique both in clinical

practice and in the research field. In AD, cortical metabolism is typically decreased in the temporoparietal cortex, the precuneus, and the posterior cingulate cortex (Herholz et al., 2002; Minoshima et al., 1997). These regions belong to the default mode network (DMN), involved in self-directed cognition. The DMN has been divided into three subsystems: the medial-temporal lobe (MTL) subsystem (including the hippocampal and parahippocampal regions), the Dorsomedial subsystem (including the dorsomedial prefrontal cortex and the temporoparietal junction) and the Midline Core subsystem (including the precuneus, the posterior cingulate cortex, and the anteromedial prefrontal cortex; Andrews-Hanna, Reidler, Sepulcre, Poulin, & Buckner, 2010). In AD, the MTL subsystem is the most affected in terms of cortical atrophy, with typical hippocampal volume reduction, whereas hypometabolism is particularly important in the core subsystem (Grothe, Teipel,, & Alzheimer's Disease Neuroimaging, 2016).

Beside the classical distribution of cortical hypometabolism, heterogeneity was frequently reported in FDG-PET among AD patients (Bokde et al., 2001; Foster et al., 1983; Kim et al., 2005; Salmon et al., 2009). With this heterogeneity in mind, the goal of the current study was to characterize a peculiar pattern of FDG-PET hypometabolism where decreased activity is prominent in the perisylvian area on visual analysis by comparison to a more typical posterior medial cortical involvement (typical pattern) in AD patients with an amnestic clinical profile.

The first step in the current study was to study a small sample of patients from the Memory Clinic, CHU Liege, to statistically confirm the visual analysis of predominant perisylvian hypometabolic pattern. The second step was to analyze clinical profiles related to the metabolic subtype in a larger group of AD patients, using the ADNI database.

2 | MATERIALS AND METHODS

2.1 | Population 1: GIGA CRC group

2.1.1 | Participants

Subjects referred to our nuclear medicine department for differential diagnosis of AD type dementia were selected based on FDG-PET visual inspection.

A first group of 31 patients was gathered because FDG-PET was characterized by a predominant posterior perisylvian hypometabolism at visual inspection. Brain CT showed predominant atrophy in the same regions. A second group (named typical), gathered over 1 year, included 25 subjects with a classical AD-like cortical hypometabolism on FDG-PET, comprising involvement of the temporoparietal and posteromedial

cortices (Herholz et al., 2002). The later participants were selected to have similar age and gender compared to the patients with major perisylvian involvement (the new temporoparietal junction or TPJ subtype). The demographic data are represented in Table 1, and t-tests show no significant difference between the typical and TPJ subtype groups in terms of age at PET time, age at first symptoms, age at diagnosis, modified Hachinski ischemic scale (MIHS) score (Hachinski, Oveisgharan, Romney, & Shankle, 2012) and mini-mental state examination (MMSE) score (Folstein, Folstein, & McHugh, 1975).

All subjects met National Institute on Aging-Alzheimer's Association clinical criteria for possible AD dementia (McKhann et al., 2011). Due to the retrospective design of this part of the study, biomarker information was limited to neurodegeneration (variable hippocampal atrophy) and patients did not have consistent neuropsychological data to be compared between groups.

For group comparison in SPM12, a control group of 12 healthy older adults without cognitive complaints consisted in participants who underwent a cerebral FDG-PET on the same scanner as the patients. The control subjects were significantly younger than the AD subjects and age was introduced as a covariate of no interest in the statistical analysis of FDG-PET.

2.1.2 | PET-scan acquisition and processing

FDG-PET scan was performed 30 min after intravenous injection of ~150 MBq of FDG using a Gemini TF or Gemini TF Big-Bore PET-CT scanner (Philips Medical Systems, Amsterdam, the Netherlands) with a 18 cm axial field of view and a 4.8 mm resolution in air. Patients had their eyes closed. A low-dose CT was acquired for attenuation correction, followed by a 12-min emission scan. The images were reconstructed using a LOR-RAMLA algorithm and corrections for attenuation, deadtime, random events, and scatter were applied. Reconstructed images had 2 mm isotropic spatial resolution and a $128 \times 128 \times 90$ matrix size.

Preprocessing and statistical analyses of FDG-PET images were conducted with SPM12 (Wellcome Centre for Human Neuroimaging, UCL, London, UK). Spatial normalization was first obtained by matching each subject's PET image to the MNI PET template provided in SPM. Those normalized images were then averaged to create an FDG-PET group-specific template smoothed with a Gaussian kernel of 8 mm full width at half maximum. This group-specific template was then used to spatially normalize patients and controls' PET images. For this classical statistical

TABLE 1 T test results studying the homogeneity of the "TPJ subtype" group and the typical group in the CRC population

	TPJ subtype (CRC)	Typical (CRC)	N TPJ	N typical	t value	Degree of freedom	p−value
Age at PET (years)	78.9 ± 6.7	78.3 ± 8.0	30	25	0.29	53	.77
Age at first symptom (years)	76.4 ± 6.9	75.3 ± 8.4	25	25	0.49	48	.62
Age at diagnosis (years)	78.7 ± 6.4	77.4 ± 8.2	30	25	0.62	53	.54
MHIS	1.33 ± 1.75	1.58 ± 1.56	30	24	−0.58	52	.59
MMSE	23.04 ± 4.18	20.90 ± 4.55	26	21	1.67	45	.10

Note: Values expressed as mean ± SD; MIHS, modified Hachinski ischemic score; MMSE, mini-mental state exam; TPJ, temporoparietal.

analysis only, normalized images underwent a smoothing with a Gaussian kernel of 12 mm full width at half maximum.

For statistical comparison, processed FDG-PET images of the three groups were entered in a General Linear Model in SPM12 using a factorial design to perform statistical comparison between the two patient groups (TPJ and typical subtypes), and healthy controls using proportional scaling by cerebral global mean values to control for FDG uptake variability. Age, mean-centered on the overall mean, was entered as a nuisance variable. The threshold for statistical significance was set at $p < .05$ with correction for multiple comparisons (FWER, family-wise error rate) at the voxel level over the whole brain volume.

2.2 | Population 2: ADNI database

2.2.1 | Selection of subjects

Variability in clinical profile associated with the two FDG-PET (classical and TPJ) subtypes observed in our initial sample was evaluated in a larger population well-characterized at the neuropsychological level, using ADNI (Alzheimer's disease neuroimaging initiative) database of AD patients (for up-to-date information, see www.adni-info.org).

All included subjects underwent the same neuropsychological tests, as well as cerebral FDG-PET. We selected all 241 mild AD patients for which a FDG-PET image was available at baseline in this database. On visual inspection, thirty-four subjects were discarded because FDG-PET images were of suboptimal quality. The FDG-PET data ($n = 207$) corresponded to the raw images recorded at their entrance in the study (ADNI1 and ADNI2 baseline). Beside neuropsychological variables, we also collected data regarding age at PET scan, gender, level of education and amyloid burden (estimated with [18F]Florbetapir PET).

Furthermore, similarly to the CRC data, the ADNI were also visually inspected and manually labeled as showing the classical AD-like cortical or the new TPJ hypometabolic profile.

2.2.2 | FDG-PET analysis

Raw FDG-PET images from ADNI database were preprocessed in SPM12 following a similar procedure as for Population 1, without smoothing.

The visually labeled data in the CRC dataset were used to construct a machine learning-based classifier to predict FDG-PET labels in the 207AD subjects from ADNI. A group-selection procedure (Wehenkel, Sutera, Bastin, Geurts, & Phillips, 2018) with 500 Extra-trees (Geurts, Ernst, & Wehenkel, 2006) based on the automated anatomical labelling (AAL) atlas (Tzourio-Mazoyer et al., 2002) was used to reduce the feature set before learning. Extra-trees are a variant of Breiman's Random forests (Breiman, 2001), which replaces bootstrap sampling in this latter method by a randomization of the discretization thresholds. This often results in improved performance (Geurts et al., 2006). The method depends on two parameters, the number T of trees in the ensemble and the number K of features drawn at each decision tree node. In all experiments in this article, T was fixed to 500 and K was set to its default value, which is the square root of the total number of input features. Our group selection procedure (Wehenkel et al., 2018) exploits variable importance

scores derived from Random forests models and random permutations to rank groups of features, corresponding in our case to brain regions from the AAL atlas (Tzourio-Mazoyer et al., 2002), according to their relevance for predicting the output class. We used the CER_r variant of this procedure with a significance threshold set to 0.05 and, for increased robustness, we retained the regions that were selected more than half of the time in 10 repetitions of 10-fold cross-validation.

Performance of the classifier was assessed by cross-validation and reverse learning. The accuracy of the CRC data based classifier was estimated through a 10 repeated 10-fold cross-validation scheme. Afterward, ADNI labels inferred from CRC data were compared to those obtained by visual inspection. Likewise, a new Extra-trees model was fitted from ADNI with the same parameters and feature reduction, then this model was tested on the GIGA CRC population. These transfer and reverse learning procedures, combined with the manually obtained labels, allowed the evaluation of the performance of the classifiers, while controlling for the potential subjectivity of human raters.

As the classifier provides class probability estimates, the performance was measured by computing the area under receiver operating characteristic (ROC) curves (AUC).

2.2.3 | Neuropsychological data

From all the information contained in the ADNI database, we selected the following tests or scales of interest that were available for all participants: Alzheimer's Disease Assessment Scale (ADAS 13), Neuropsychiatric Inventory (NPI), Clinical Dementia Rating Scale (CDR), Mini Mental State Exam (MMSE), Rey Auditory-Verbal Learning Test (RAVLT), animal fluency, Trail Making Test (TMT A and B), Logical Memory immediate and delayed recall, and the Boston Naming Test (BNT). Data from Digit Span and vegetable fluency were not selected because of too many missing values.

Using the labels predicted from the classifier (trained on the first population to predict the label in the second one), machine learning was used to construct a new model discriminating between the two AD groups, based on neuropsychological scores. In order to have good interpretability of the problem, the model chosen was a Random forests ensemble (Extra-trees). The analysis of variable importance scores derived from this model (Louppe, Wehenkel, & Geurts, 2013) enabled the identification of the most relevant neuropsychological scores to differentiate the two groups. Importance scores were averaged over 10 repeats to obtain this ranking. Posthoc Student t-test was used to confirm between-group differences that had clinical meaning.

2.2.4 | Interregional correlations in FDG-PET data in the ADNI population

In order to better characterize the cerebral networks affected in the two groups of subjects, SPM12 multiple regression was used to search for interregional metabolic correlations, between peak voxel values of the most discriminant regions obtained in our first population (left precuneus and left temporoparietal junction reported in Table 2, taken as seed regions) and FDG-PET metabolism in the other regions of the brain, in the ADNI population. The threshold for statistical significance was set at

$p < .05$ with correction for multiple comparisons (FWER, family-wise error rate) at the voxel level for the whole brain.

3 | RESULTS

3.1 | FDG-PET statistical analysis in Population 1 (GIGA CRC group)

The results of the SPM12 group comparisons are summarized in Table 2. When each group was separately compared to the control group, both AD types showed a significant decrease of metabolic activity in the left precuneus (Figure 1). The direct comparison between the typical and the TPJ subtype group (with perisylvian involvement) revealed that the typical subjects showed significant hypometabolism in the left precuneus and the right inferior temporal cortex compared to the TPJ subtype, whereas the TPJ subtype subjects showed a significant decrease of metabolic activity in the temporoparietal junction compared to typical subjects (Figure 2). This analysis thereby statistically confirmed and specified the visual inspection.

3.2 | Population 2: Classification of ADNI FDG-PET data and analysis of clinical profiles

3.2.1 | Classification of subjects

The feature selection procedure highlighted 11 relevant regions of interest for subsequent classification (the left rolandic operculum, the

TABLE 2 MNI coordinates of the different regions showing hypometabolism in FDG-PET

	Region	x	y	z	Cluster size
1.Typical (<control)	Left precuneus	−15	−55	73	4,141
2. Atypical (<control)	Left precuneus	−15	−55	76	1,601
3.Typical (<atypical)	Left precuneus	−3	−46	46	104
	Right latero-inferior temporal cortex	57	−52	−11	30
4. Atypical (<typical)	Left TPJ	60	−4	7	229

Note: $p < .05$ FWER corrected.

TABLE 3 T test results studying the homogeneity of the "TPJ subtype" group and the "typical" group in the ADNI population

	TPJ subtype (ADNI)	Typical (ADNI)	N TPJ	N typical	t value	Degree of freedom	p−value
Age at PET	77.47 ± 7.73	72.84 ± 7.59	78	129	−4.27	202	< .001
Level of education	15.26 ± 3.12	15.47 ± 2.64			0.52		.09

Note: Values expressed as mean ± SD.
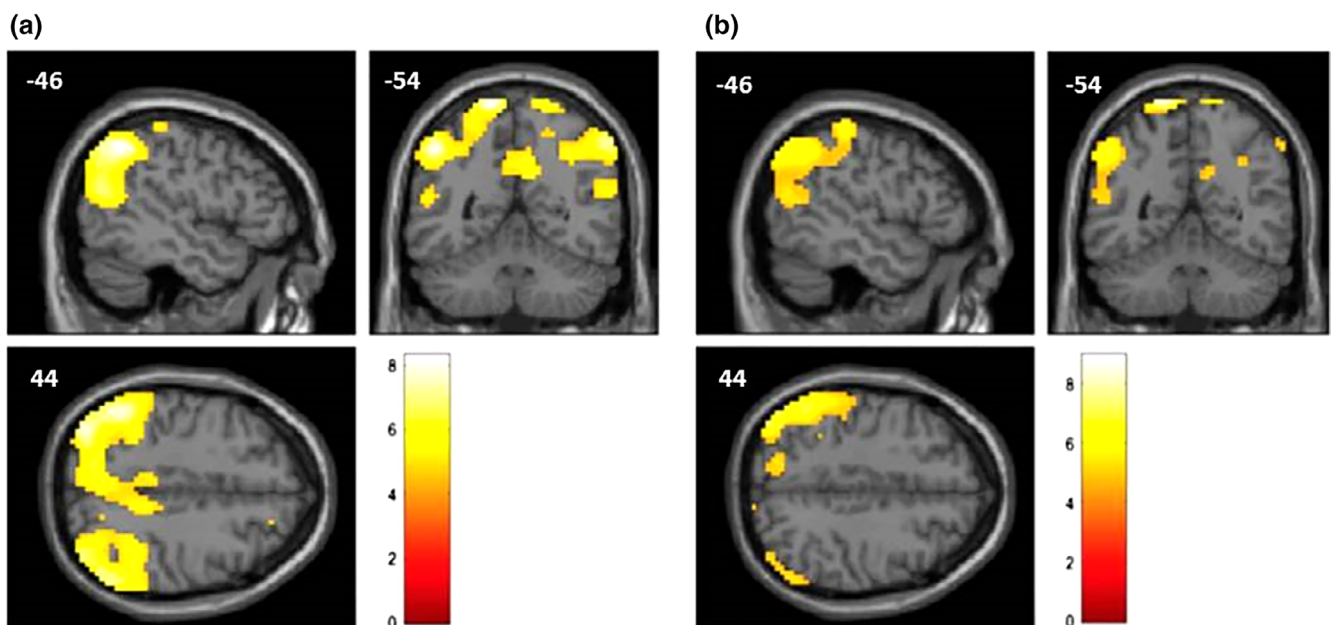
FIGURE 1 Representation, on a standard structural magnetic resonance (MR) image, of the cortical regions showing a significant metabolic decrease (measured with FDG-PET) in the typical group (a) and the TPJ subtype group (b) compared to the control group, using the age as a nuisance variable. The regions, represented in the MNI space, are mostly posterior associative cortices. Color scale represents t-value ((a, degree of freedom = 36; b, degree of freedom = 42)

(a)

(b)
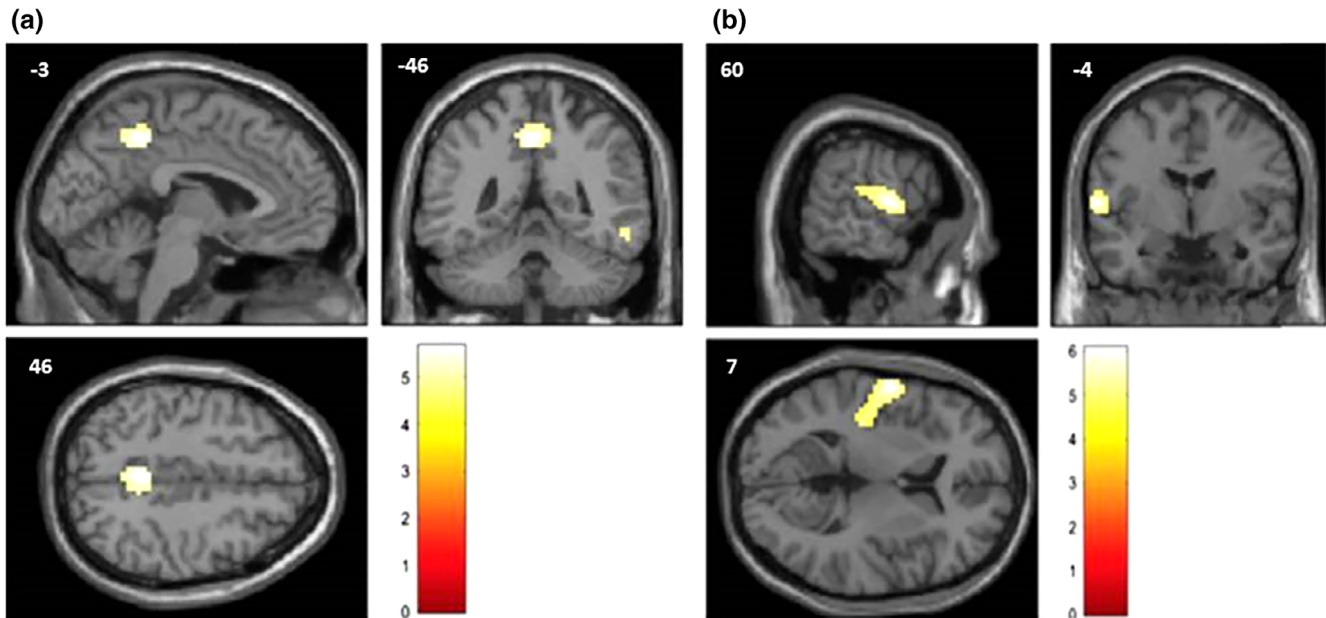
FIGURE 2 (a) Representation, on a standard structural MRI, of the cortical regions showing a significant metabolic decrease in the typical group compared to the TPJ subtype group, using the age as a nuisance variable. The regions, represented in the MNI space, are mostly the precuneus and the right latero-inferior temporal cortex. (Table 2). (b) Representation, on a standard structural MRI, of the cortical regions showing a significant metabolic decrease in the TPJ subtype group compared to the typical group, using the age as a nuisance variable. The region, represented in the MNI space, is mostly the parieto-temporal junction. (Table 2). Color scale represents *t*-value (degree of freedom = 55)

superior parietal gyri, the right angular gyrus, the bilateral precuneus, the Heschl gyri, the left superior temporal gyrus, the right middle temporal gyrus, and the right inferior temporal gyri)), based on the AAL (Tzourio-Mazoyer et al., 2002). We thus reduced our feature set to only these regions and fitted an ensemble of 500 Extra-trees on the learning set. The cross-validation assessment of this selection and classification on the GIGA-CRC data lead to an area under the curve of 71.73% (±2.87%).

Using only these regions of interest, the classifier was able to distinguish two groups in the ADNI population similar to the initial two subtypes observed in the GIGA CRC data. Out of 207 subjects, the percentage of TPJ subtype subjects was 38% (78 participants, while 129 subjects FDG-PET were labeled as typical). The comparison between this prediction and the manually labeled ADNI data showed an area under the curve value of 82.52% (±0.48%). This shows a good level of consistency between the two approaches, transfer learning and manual labelling, even though there is no "ground truth" available.

Using the reverse learning method with the CRC population, the area under the curves showed 86.11% (± 0.36%) accuracy of our classifier.

Considering the labels defined by the classifier, the TPJ subtype subjects from the ADNI population were significantly older than typical subjects (*p* < .001) but did not differ in terms of level of education or MMSE (Table 3). The proportion of amyloid positive PET was similar in both groups (62% in TPJ, 77% in typical patients, chi-square 2.344, *p* = .126), with the limitation that only half of the subjects underwent a [18F]Florbetapir PET.

3.2.2 | Neuropsychological results

Machine learning was used to construct a model discriminating one group from the other, based on neuropsychological scores. In this model, the features are the neuropsychological scores and the corresponding output is the group of the AD patient previously predicted by the classifier model. The only test that consistently occupied the first position throughout the 10 repeats from the Extra-trees model was the TMT-A (time of completion). The importance of this test to discriminate between the subjects was further confirmed with a *t*-test, and TMT-A response times was significantly faster in the TPJ subtype group (M = 57.97 s, SD = 29.2) than in the typical group (M = 73.23 s, SD = 40.17; *t* [203] = 2.99, *p* < .005). This was confirmed when performing correction for multiple comparisons of the scores selected in Section 2.2.3.

3.2.3 | Interregional correlations in FDG-PET

In the typical group, activity in the left precuneus (seed: x = −3, y = −46, z = 46) mostly significantly correlated with metabolism in parietal and premotor regions (Figure 3a). In the TPJ subtype, activity in the left temporoparietal junction (seed: x = −60, y = −4, z = 7) essentially correlated with metabolism in perisylvian regions (Figure 3b).

4 | DISCUSSION

In this study, we report a new metabolic subtype with decreased glucose metabolism (and atrophy) predominant in the perisylvian region,

(a)

(b)
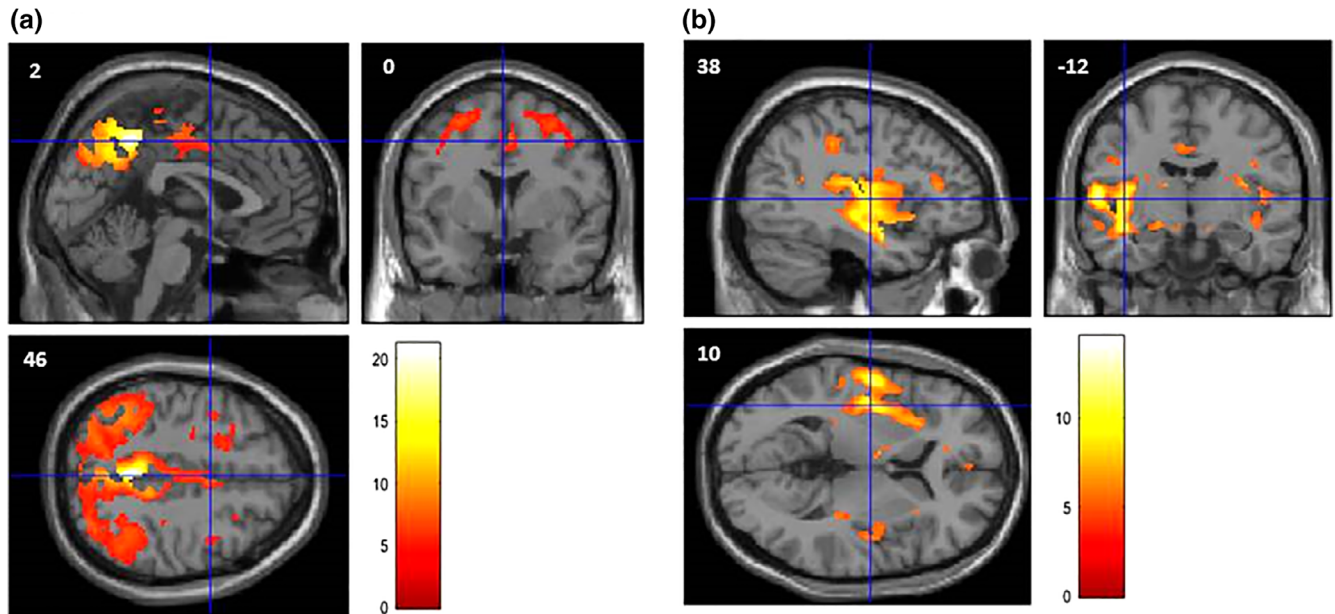
FIGURE 3 Interregional metabolic correlations, between peak voxel values of the most discriminant regions taken as "seed regions" (obtained in the GIGA-CRC population) and metabolism in the other regions of the brain, in the ADNI population, with *p*-value <.05 (FWER corrected). MNI space. Color scale represents *t*-value (degree of freedom = 205). (a) In the "Typical" group, activity in the left precuneus correlates with metabolism in parietal and premotor regions. (b) In the "TPJ subtype" group, activity in the left temporoparietal junction correlates with metabolism in perisylvian regions

that could be referred to as temporoparietal junction (TPJ) subtype. Initially detected by visual inspection in patients from a clinical sample, significant differences in metabolic activity between this subtype (TPJ hypometabolism) and a more typical group with predominant hypometabolism of the posteromedial cortex were confirmed using SPM12. A Extra-trees classifier was then constructed based on this first analysis and was applied to an ADNI population. With this classifier, we were able to label 78 ADNI AD patients as TPJ subtypes out of 207 subjects with a probable mild AD diagnosis, with high accuracy level (85.84% of correct labelling with a reverse learning method). Accordingly, the TPJ subtype observed in about 38% of ADNI amnestic AD patients appears as a consistent variant of the typical FDG-PET profile.

Heterogeneity of regional brain pathology is well-documented in AD. Subtypes have been described from a neuropathological viewpoint, with the observation of typical, limbic, and cortical subtypes (Murray et al., 2011) and with the description of Alzheimer's pathology in atypical clinical presentations (Alladi et al., 2007; Galton et al., 2000). These neuropathological presentations correlate with the heterogeneity observed in neuroimaging studies with MRI (Ridgway et al., 2012; Whitwell et al., 2012) or FDG-PET (Bokde et al., 2001; Foster et al., 1983; Kim et al., 2005). Based on these findings of heterogeneity, AD is currently seen as a wide spectrum with different clinical and neuropsychological presentations (amnestic, posterior cortical atrophy, progressive primary aphasia, and frontal variants) that are reflected in imaging and neuropathological studies (Galton et al., 2000; McKhann et al., 2011; Murray et al., 2011). These correlations have also been studied in the early onset presentation of the disease:

typical amnestic early-onset AD, logopenic progressive aphasia and posterior cortical atrophy were associated with disease-specific reductions in cortical thickness (Ridgway et al., 2012).

Clinical and neuropsychological heterogeneity has also been associated with different patterns of cortical hypometabolism. Different networks are specifically involved depending on the neuropsychological presentation. Although the Default Mode Network (DMN) is involved in all AD subtypes, focal patterns of hypometabolism characterize each variant: the left temporoparietal cortex in the logopenic variant, the ventral DMN in the early-onset or the bilateral prefrontal cortex in the executive/frontal variants (Lehmann et al., 2013; Vanhoutte et al., 2017).

Even if both regions belong to the DMN, predominant TPJ and posteromedial hypometabolism do not seem to reflect variants of a same network breakdown. Indeed, with seed-based interregional correlation analysis previously used to reveal metabolic patterns in AD (Lehmann et al., 2013; Seeley, Crawford, Zhou, Miller, & Greicius, 2009), we found a predominant correlation of the metabolism of the left precuneus with parietal and premotor regions in the typical group, and a prominent correlation between the metabolism of the left TPJ and that of perisylvian regions in the TPJ subtype. The TPJ subtype was not characterized by severe medial temporal involvement or by relative sparing of the hippocampus compared to the typical subtype (Ferreira et al., 2017; Murray et al., 2011). It cannot be considered as a diffuse involvement of associative cortices (Noh et al., 2014; Park et al., 2017) or as a group with no atrophy (Ferreira et al., 2017).

ADNI data allowed examining whether these different metabolic profiles are associated with distinct clinical presentations. Actually,

the two groups (typical and TPJ subtype) could only be distinguished by age (i.e., TPJ subtype patient being older) and by very few, non-memory neuropsychological tests such as TMT-A, with faster response time in the TPJ subtype group compared to the typical sub-type group. As TMT-A test mainly involves visuomotor and attention abilities, we could assume that these abilities are more affected in the typical group. Interestingly, in an fMRI study, brain activity was observed in motor, premotor, and visual areas in healthy subjects per-forming a TMT-A task (Karimpoor et al., 2017). Therefore, the meta-bolic connectivity we described between premotor regions and metabolically impaired left precuneus in the typical group could partic-ipate to their lower performance at this test. Nevertheless, apart from this difference, patients from the two types could not be clearly dis-tinguished in terms of cognitive or neuropsychiatric profile. Clinically, they were all found to fulfill the clinical diagnosis of amnestic AD (McKhann et al., 2011). Moreover, compared to healthy older partici-pants, they all demonstrated reduced metabolism in the precuneus. Also, most of the patients had significant amyloid burden on PET in both groups. Yet, the prominent cortical site of neurodegeneration varied between them.

5 | CONCLUSION

The current findings suggest that a relatively comparable clinical pre-sentation in AD can be accompanied by a typical FDG-PET pattern or by a clearly distinct metabolic TPJ subtype, although one cannot exclude that current clinical evaluation was not sensitive enough to differentiate the two groups.

ORCID

Eric Salmon https://orcid.org/0000-0003-2520-9241

REFERENCES

Alladi, S., Xuereb, J., Bak, T., Nestor, P., Knibb, J., Patterson, K., & Hodges, J. R. (2007). Focal cortical presentations of Alzheimer's dis-ease. *Brain*, *130*(Pt 10), 2636–2645. https://doi.org/10.1093/brain/awm213

Andrews-Hanna, J. R., Reidler, J. S., Sepulcre, J., Poulin, R., & Buckner, R. L. (2010). Functional-anatomic fractionation of the brain's default net-work. *Neuron*, *65*(4), 550–562. https://doi.org/10.1016/j.neuron.2010.02.005

Bokde, A. L., Pietrini, P., Ibanez, V., Furey, M. L., Alexander, G. E., Graff-Radford, N. R., ... Horwitz, B. (2001). The effect of brain atrophy on cerebral hypometabolism in the visual variant of Alzheimer disease. *Archives of Neurology*, *58*(3), 480–486.

Breiman, L. (2001). Random forests. *Machine Learning*, *45*(1), 5–32.

Ferreira, D., Verhagen, C., Hernandez-Cabrera, J. A., Cavallin, L., Guo, C. J., Ekman, U., ... Westman, E. (2017). Distinct subtypes of Alzheimer's dis-ease based on patterns of brain atrophy: Longitudinal trajectories and clinical applications. *Scientific Reports*, *7*, 46263. https://doi.org/10.1038/srep46263

Fisher, N. J., Rourke, B. P., & Bieliauskas, L. A. (1999). Neuropsychological subgroups of patients with Alzheimer's disease: An examination of the first 10 years of CERAD data. *Journal of Clinical and Experimental Neuro-psychology*, *21*(4), 488–518. https://doi.org/10.1076/jcen.21.4.488.887

Folstein, M. F., Folstein, S. E., & McHugh, P. R. (1975). "mini-mental state". A practical method for grading the cognitive state of patients for the clinician. *Journal of Psychiatric Research*, *12*(3), 189–198.

Foster, N. L., Chase, T. N., Fedio, P., Patronas, N. J., Brooks, R. A., & Di Chiro, G. (1983). Alzheimer's disease: Focal cortical changes shown by positron emission tomography. *Neurology*, *33*(8), 961–965.

Frisoni, G. B., Testa, C., Sabattoli, F., Beltramello, A., Soininen, H., & Laakso, M. P. (2005). Structural correlates of early and late onset Alzheimer's disease: Voxel based morphometric study. *Journal of Neu-rology, Neurosurgery, and Psychiatry*, *76*(1), 112–114. https://doi.org/10.1136/jnnp.2003.029876

Galton, C. J., Patterson, K., Xuereb, J. H., & Hodges, J. R. (2000). Atypical and typical presentations of Alzheimer's disease: A clinical, neuropsy-chological, neuroimaging and pathological study of 13 cases. *Brain*, *123*(Pt 3), 484–498.

Geurts, P., Ernst, D., & Wehenkel, L. (2006). Extremely randomized trees. *Machine Learning*, *63*, 3–42.

Grothe, M. J., Teipel, S. J., & Alzheimer's Disease Neuroimaging Initiative. (2016). Spatial patterns of atrophy, hypometabolism, and amyloid deposition in Alzheimer's disease correspond to dissociable functional brain networks. *Human Brain Mapping*, *37*(1), 35–53. https://doi.org/10.1002/hbm.23018

Hachinski, V., Oveisgharan, S., Romney, A. K., & Shankle, W. R. (2012). Optimizing the Hachinski ischemic scale. *Archives of Neurology*, *69*(2), 169–175. https://doi.org/10.1001/archneurol.2011.1698

Herholz, K., Salmon, E., Perani, D., Baron, J. C., Holthoff, V., Frolich, L., … Heiss, W. D. (2002). Discrimination between Alzheimer dementia and controls by automated analysis of multicenter FDG PET. *NeuroImage*, *17*(1), 302–316.

Jack, C. R., Jr., Bennett, D. A., Blennow, K., Carrillo, M. C., Feldman, H. H., Frisoni, G. B., … Dubois, B. (2016). A/T/N: An unbiased descriptive classification scheme for Alzheimer disease biomarkers. *Neurology*, *87*(5), 539–547. https://doi.org/10.1212/WNL.0000000000002923

Karch, C. M., & Goate, A. M. (2015). Alzheimer's disease risk genes and mechanisms of disease pathogenesis. *Biological Psychiatry*, *77*(1), 43–51. https://doi.org/10.1016/j.biopsych.2014.05.006

Karimpoor, M., Churchill, N. W., Tam, F., Fischer, C. E., Schweizer, T. A., & Graham, S. J. (2017). Tablet-based functional MRI of the trail making test: Effect of tablet interaction mode. *Frontiers in Human Neuroscience*, *11*, 496. https://doi.org/10.3389/fnhum.2017.00496

Kim, E. J., Cho, S. S., Jeong, Y., Park, K. C., Kang, S. J., Kang, E., … Na, D. L. (2005). Glucose metabolism in early onset versus late onset Alzheimer's disease: An SPM analysis of 120 patients. *Brain*, *128*(Pt 8), 1790–1801. https://doi.org/10.1093/brain/awh539

Lambon, R.,, M. A., Patterson, K., Graham, N., Dawson, K., & Hodges, J. R. (2003). Homogeneity and heterogeneity in mild cognitive impairment and Alzheimer's disease: A cross-sectional and longitudinal study of 55 cases. *Brain*, *126*(Pt 11), 2350–2362. https://doi.org/10.1093/brain/awg236

Lehmann, M., Ghosh, P. M., Madison, C., Laforce, R., Jr., Corbetta-Rastelli, C., Weiner, M. W., … Rabinovici, G. D. (2013). Diverging patterns of amyloid deposition and hypometabolism in clinical variants of probable Alzheimer's disease. *Brain*, *136*(Pt 3), 844–858. https://doi.org/10.1093/brain/aws327

Louppe, G., Wehenkel, L.,, A.,, S., & Geurts, P. (2013). Understanding variable importances in forests of randomized trees. In C. J. C. Burges, L. Bottou, M. Welling, Z. Ghahramani, & K. Q. Weinberger (Eds.), *Advances in neural information processing systems 26 (NIPS 2013)* (Vol. 26, pp. 431–439). NY: Curran Associates, Inc.

McKhann, G. M., Knopman, D. S., Chertkow, H., Hyman, B. T., Jack, C. R., Jr., Kawas, C. H., … Phelps, C. H. (2011). The diagnosis of dementia due to Alzheimer's disease: Recommendations from the National Institute on Aging-Alzheimer's Association workgroups on diagnostic guidelines for Alzheimer's disease. *Alzheimers Dement*, *7*(3), 263–269. https://doi.org/10.1016/j.jalz.2011.03.005

Minoshima, S., Giordani, B., Berent, S., Frey, K. A., Foster, N. L., & Kuhl, D. E. (1997). Metabolic reduction in the posterior cingulate cortex in very early Alzheimer's disease. *Annals of Neurology*, *42*(1), 85–94. https://doi.org/10.1002/ana.410420114

Murray, M. E., Graff-Radford, N. R., Ross, O. A., Petersen, R. C., Duara, R., & Dickson, D. W. (2011). Neuropathologically defined subtypes of Alzheimer's disease with distinct clinical characteristics: A retrospective study. *Lancet Neurology*, *10*(9), 785–796. https://doi.org/10.1016/S1474-4422(11)70156-9

Noh, Y., Jeon, S., Lee, J. M., Seo, S. W., Kim, G. H., Cho, H., … Na, D. L. (2014). Anatomical heterogeneity of Alzheimer disease: Based on cortical thickness on MRIs. *Neurology*, *83*(21), 1936–1944. https://doi.org/10.1212/WNL.0000000000001003

Park, J. Y., Na, H. K., Kim, S., Kim, H., Kim, H. J., Seo, S. W., … Alzheimer's Disease Neuroimaging Initiative. (2017). Robust identification of Alzheimer's disease subtypes based on cortical atrophy patterns. *Scientific Reports*, *7*, 43270. https://doi.org/10.1038/srep43270

Ridgway, G. R., Lehmann, M., Barnes, J., Rohrer, J. D., Warren, J. D., Crutch, S. J., & Fox, N. C. (2012). Early-onset Alzheimer disease clinical variants: Multivariate analyses of cortical thickness. *Neurology*, *79*(1), 80–84. https://doi.org/10.1212/WNL.0b013e31825dce28

Salmon, E., Kerrouche, N., Perani, D., Lekeu, F., Holthoff, V., Beuthien-Baumann, B., … Herholz, K. (2009). On the multivariate nature of brain metabolic impairment in Alzheimer's disease. *Neurobiology of Aging*, *30*(2), 186–197.

Seeley, W. W., Crawford, R. K., Zhou, J., Miller, B. L., & Greicius, M. D. (2009). Neurodegenerative diseases target large-scale human brain networks. *Neuron*, *62*(1), 42–52. https://doi.org/10.1016/j.neuron.2009.03.024

Stopford, C. L., Snowden, J. S., Thompson, J. C., & Neary, D. (2008). Variability in cognitive presentation of Alzheimer's disease. *Cortex*, *44*(2), 185–195. https://doi.org/10.1016/j.cortex.2005.11.002

Strite, D., Massman, P. J., Cooke, N., & Doody, R. S. (1997). Neuropsychological asymmetry in Alzheimer's disease: Verbal versus visuoconstructional deficits across stages of dementia. *Journal of the International Neuropsychological Society*, *3*(5), 420–427.

Tzourio-Mazoyer, N., Landeau, B., Papathanassiou, D., Crivello, F., Etard, O., Delcroix, N., … Joliot, M. (2002). Automated anatomical labeling of activations in SPM using a macroscopic anatomical parcellation of the MNI MRI single-subject brain. *NeuroImage*, *15*(1), 273–289. https://doi.org/10.1006/nimg.2001.0978

Vanhoutte, M., Semah, F., Rollin Sillaire, A., Jaillard, A., Petyt, G., Kuchcinski, G., … Lopes, R. (2017). (18)F-FDG PET hypometabolism patterns reflect clinical heterogeneity in sporadic forms of early-onset Alzheimer's disease. *Neurobiology of Aging*, *59*, 184–196. https://doi.org/10.1016/j.neurobiolaging.2017.08.009

Vardy, E. R., Ford, A. H., Gallagher, P., Watson, R., McKeith, I. G., Blamire, A., & O'Brien, J. T. (2013). Distinct cognitive phenotypes in Alzheimer's disease in older people. *International Psychogeriatrics*, *25*(10), 1659–1666. https://doi.org/10.1017/S1041610213000914

Wehenkel, M., Sutera, A., Bastin, C., Geurts, P., & Phillips, C. (2018). Random forests based group importance scores and their statistical interpretation: Application for Alzheimer's disease. *Frontiers in Neuroscience*, *12*, 411. https://doi.org/10.3389/fnins.2018.00411

Whitwell, J. L., Dickson, D. W., Murray, M. E., Weigand, S. D., Tosakulwong, N., Senjem, M. L., … Josephs, K. A. (2012). Neuroimaging correlates of pathologically defined subtypes of Alzheimer's disease: A case-control study. *Lancet Neurology*, *11*(10), 868–877. https://doi.org/10.1016/S1474-4422(12)70200-4